

Influence of spectral phase on cross-polarized wave generation with short femtosecond pulses

L. Canova · O. Albert · N. Forget · B. Mercier ·
S. Kourtev · N. Minkovski · S.M. Saltiel ·
R. Lopez Martens

Received: 22 May 2008 / Revised version: 3 July 2008 / Published online: 10 September 2008
© Springer-Verlag 2008

Abstract In this paper we present the first comprehensive study of the role of spectral phase on cross-polarized wave (XPW) generation using sub-30 femtosecond (fs) laser pulses. XPW generation improves the temporal contrast and shortens the pulse duration of fs chirped pulse amplification (CPA) lasers. For Ti:Sa lasers, compression below 30 fs is non-trivial and therefore never perfect. We therefore systematically analyze the effect of an arbitrary input spectral phase on the output spectrum and efficiency of the XPW process, both theoretically and experimentally. We derive the maximum acceptable value of residual phase for a given initial pulse duration in order to efficiently drive the XPW process for pulse shortening and contrast improvement.

PACS 06.60.Jn · 42.65.Re

1 Introduction

Cross-Polarized Wave (XPW) generation is a direct achromatic $\chi^{(3)}$ process in cubic crystals where an intense linearly polarized incident wave can generate a new linearly polarized wave in the orthogonal direction [1]. XPW generation has demonstrated its ability to filter amplified spontaneous emission (ASE) out of a high power femtosecond

pulse, thereby increasing its temporal contrast [2–4]. When used in a double chirped pulse amplification configuration, XPW is a practical way of generating high-peak power femtosecond pulses with high contrast (typically better than $>10^{10}:1$ at the 100 TW peak power level), a prerequisite for performing relativistic laser-solid target interactions. Reducing the pulse duration in CPA lasers is an alternative way of reaching higher peak-powers without increasing the overall pulse energy. XPW features among the efficient methods proposed for overcoming gain narrowing in Ti:Sa CPA lasers and bringing the output pulse duration below the 30 fs barrier [2, 5–9].

Compared to second harmonic generation, XPW is automatically phase matched and, below saturation, only the input spectral phase influences the generated output spectrum. The effect of a pure second order phase on the XPW spectrum has been discussed in [10]. It was shown that, in the case of zero second order phase and when neglecting higher order phase terms, the XPW spectrum is broader by a factor $\sqrt{3}$ with respect to the initial spectrum. Any residual second order spectral phase reduces the spectral broadening and the XPW spectrum can even become $1/\sqrt{3}$ narrower for large values of second order phase. This analysis has demonstrated that efficient XPW filtering has to be implemented with well compressed pulses within a double CPA configuration [11]. With the growing need for intense ultrashort pulses with ultra-high contrast ($>10^{12}:1$ at the PetaWatt level) it is important to extend the XPW technique to the range of pulse durations comprised between 10 and 30 fs. For such pulses the presence of residual higher order spectral phase terms after the first pulse compression stage can no longer be neglected and it is important to quantify their effect on the XPW spectrum and efficiency. A measure of fs pulse compression can be obtained using SPIDER and FROG temporal characterization techniques. For

L. Canova · O. Albert (✉) · B. Mercier · R. Lopez Martens
Laboratoire d'Optique Appliquée, ENSTA Paristech, Ecole
Polytechnique, CNRS UMR7639, 91761 Palaiseau Cedex, France
e-mail: Olivier.Albert@ensta.fr

N. Forget
Fastlite, École Polytechnique bât. 403, 91128 Palaiseau, France

S. Kourtev · N. Minkovski · S.M. Saltiel
Faculty of Physics, University of Sofia, 5 J. Bourchier Boulevard,
1164 Sofia, Bulgaria

a 30 fs pulse, typical measurement precision for second- and third-order spectral phase is on the order of 100 fs^2 and 10000 fs^3 [12–14]. In this paper, we demonstrate that within this window of residual spectral phase, the XPW spectrum can change considerably, especially in the presence of residual higher orders phase. We show quantitatively how to account for this residual phase in order to obtain an ultra-short, high contrast pulse with a broad Gaussian spectrum, which is ideally suited either for direct use in experiments or for further amplification to higher peak powers.

The paper is organized as follows: in a theoretical introduction we define the spectral parameters we use to describe the role of spectral phase on XPW generation process and we solve the XPW equations within the approximation of non depletion of the input pulse. Within the approximation of the stationary phase, we derive an analytical model that predicts, in a simple way, the position for the maximum of the XPW spectrum for an input pulse with arbitrary spectral phase. We then treat the problem numerically to obtain more general results. Finally, we present the experimental results and compare them with calculations.

2 Theoretical considerations

2.1 Notations

For practical reasons linked to the fact that the XPW process leads to a strong pulse reshaping, we chose to characterize the XPW spectrum by its statistic moments rather than central wavelength and FWHM spectral width. We therefore use the following formulas to evaluate, respectively, the energy, spectral width, and center of mass of a given spectral distribution $I(\omega)$:

$$E_I = \int_{\mathbb{R}} I(\omega) d\omega, \quad (1)$$

$$\sigma_I^2 = \frac{\int_{\mathbb{R}} (\omega - \langle \omega \rangle_I)^2 I(\omega) d\omega}{\int_{\mathbb{R}} I(\omega) d\omega}, \quad \langle \omega \rangle_I = \frac{\int_{\mathbb{R}} \omega I(\omega) d\omega}{\int_{\mathbb{R}} I(\omega) d\omega}.$$

These parameters are not only universal and easy to define but also of first interest from an experimental point of view: the efficiency of the nonlinear process defines the energy at the output of the filter, the standard deviation defines the minimum available transform limited pulse duration and the spectral center of mass shift indicates whether the XPW spectrum still lies in the amplification bandwidth of a laser amplifier. More generally, we also define the mean value of the spectral function $f(\omega)$ with respect to the intensity $I(\omega)$ by:

$$\langle f(\omega) \rangle_I = \frac{\int_{\mathbb{R}} f(\omega) I(\omega) d\omega}{\int_{\mathbb{R}} I(\omega) d\omega}. \quad (2)$$

2.2 Propagation equation

The effect of spectral phase on a nonlinear process has been extensively studied theoretically for $\chi^{(2)}$ processes [15–19]. We extend this study to $\chi^{(3)}$ processes and, more specifically, to XPW generation. This study can be used for the description of any degenerated four wave mixing nonlinear process.

XPW generation is a degenerated third order nonlinear process. It occurs in any nonlinear medium whose third order nonlinear susceptibility is anisotropic [1] and it allows the conversion of an input linearly polarized wave into an orthogonally polarized wave. We consider the plane wave propagation equations describing the XPW generation of a linearly polarized pulse when a cubic crystal is illuminated by a short, intense and orthogonally polarized input pulse. For the sake of clarity, we neglect all dispersion and absorption effects as well as all non linear effects (self and cross-phase modulations, four-wave mixing processes, ...) other than XPW generation process. As in [10], we use the following notations: ω_0 stands for the central angular frequency of the input pulse (fundamental pulse), n_0 for the refractive index of the cubic crystal at ω_0 , $\chi^{(3)}$ for the third order susceptibility tensor, σ_χ for the anisotropy factor of this tensor, β for the angle between the input polarization direction and the crystallographic axis X, $A(z, t)$ and $B(z, t)$ for the respective complex amplitude envelopes of the fundamental and XPW electric fields, $I_A(z, \omega)$ and $I_B(z, \omega)$ for the respective spectral intensity of the fundamental and XPW electric fields. The spectral phase function of the fundamental pulse will be referred as $\varphi(\omega)$ and, when required, $\varphi(\omega)$ will be expanded in a Taylor series around ω_0 :

$$\varphi(\omega) = \sum_{k=0}^n \frac{\varphi^{(k)}}{k!} (\omega - \omega_0)^k, \quad (3)$$

where $\varphi^{(2)}$ is the linear chirp and $\varphi^{(3)}$ the quadratic chirp.

In the frame of the moving pulse, the slowly varying envelope approximation leads to the following propagation equation for the complex amplitude of the XPW field:

$$\frac{\partial B(z, t)}{\partial z} = i\gamma_\perp A(z, t)A^*(z, t)A(z, t) \quad (4)$$

$$\text{with } \gamma_\perp = -\frac{3}{8} \frac{\omega_0}{n_0 c} \chi_{xxxx}^{(3)} \frac{\sigma_\chi}{4} \sin(4\beta). \quad (5)$$

Using the standard Fourier transform $B(z, t) = \int_{\mathbb{R}} \hat{B}(z, \omega) \exp(i\omega t) d\omega$ and $A(z, t) = \int_{\mathbb{R}} \hat{A}(z, \omega) \exp(i\omega t) d\omega$ and applying the reverse convolution theorem we obtain the following equation for the complex spectral amplitude of the XPW pulse:

$$\begin{aligned} & \frac{\partial \hat{B}(z, \omega)}{\partial z} \\ &= -i\gamma_{\perp} \iint_{\mathbb{R}^2} \hat{A}(z, \omega_1) \hat{A}(z, \omega_2) \hat{A}^* \\ & \quad \times (z, \omega_1 + \omega_2 - \omega) d\omega_1 d\omega_2. \end{aligned} \tag{6}$$

Equation (6) enlightens the frequency-mixing process occurring in the XPW generation: the XPW signal at a given angular frequency is proportional to some third order spectral autocorrelation function of the fundamental pulse. In the approximation of small conversion efficiency (undepleted regime) and of negligible dispersion, the fundamental pulse propagates unchanged ($A(z, t) = A(0, t) = A(t)$) and (6) can be solved analytically:

$$\begin{aligned} & \hat{B}(L, \omega) \\ &= -i\gamma_{\perp} L \iint_{\mathbb{R}^2} \hat{A}(\omega_1) \hat{A}(\omega_2) \hat{A}^*(\omega_1 + \omega_2 - \omega) d\omega_1 d\omega_2. \end{aligned} \tag{7}$$

2.3 Gaussian pulse with quadratic phase

For a fundamental pulse of Gaussian spectral intensity, the spectral amplitude is:

$$\hat{A}(\omega) = \hat{A}_0 \exp\left(-\frac{(\omega - \omega_0)^2}{2\sigma^2}\right) \exp[i\varphi(\omega)] \tag{8}$$

with the spectral phase defined as in (3). The right hand side of (7) can be solved analytically for the specific case of a quadratic phase. The result for the spectral intensity in this case is:

$$\begin{aligned} & I_B(L, \omega) \\ &= (2\pi\sigma^2 \hat{A}_0^3 \gamma_{\perp} L)^2 \frac{\exp[-\frac{(\omega - \omega_0)^2}{3\sigma^2} \frac{(1 + \sigma^4(\varphi^{(2)})^2)}{(1 + \sigma^4(\varphi^{(2)})^2/9)}]}{\sqrt{(1 + \sigma^4(\varphi^{(2)})^2)(9 + \sigma^4(\varphi^{(2)})^2)}}. \end{aligned} \tag{9}$$

This analytical result shows that for Fourier-transform limited input pulse ($\varphi^{(2)} = 0$) the XPW spectrum is $\sqrt{3}$ times broader than the input pulse. For chirped pulses ($\varphi^{(2)} \neq 0$) however, the XPW spectral width narrows with increasing $\varphi^{(2)}$ and is $1/\sqrt{3}$ smaller than input spectrum for a high spectral chirp. Integrating (9) over the frequency domain, one can also obtain the dependence of the XPW pulse energy, on the input second order spectral phase coefficient $\varphi^{(2)}$:

$$E_{XPW}(L, \varphi^{(2)}) = \frac{E_{XPW,0}}{(1 + \sigma^4(\varphi^{(2)})^2)}, \tag{10}$$

where $E_{XPW,0}$ is the XPW energy of the pure Fourier transform limited pulse. As can be seen, this dependence is Lorentzian. From (9) we can also calculate the spectral center of mass. Applying (1) leads to $\langle \omega \rangle_{XPW} = \omega_0$, demonstrating that there is no spectral shift.

From the previous results, one can define two critical second order coefficient values corresponding, respectively, to the following conditions: the XPW efficiency is equal to half of the maximum conversion efficiency, the XPW spectrum is equal to the input spectrum. For a Gaussian input pulse, these critical coefficients are given by:

$$\varphi_{cr,Energy}^{(2)} = \sqrt{3}/\sigma^2, \tag{11}$$

$$\varphi_{cr,Width}^{(2)} = 1/\sigma^2. \tag{12}$$

For a Gaussian pulse of minimal pulse duration $\tau_0 = 30$ fs the spectral width at $1/e$ is $\sigma = 55.5$ THz and the corresponding critical second order phase coefficients are 325 and 562 fs², respectively.

If we consider the more general case of an input polynomial phase, the integration in (6) needs to be performed numerically. This is presented in Sect. 2.5. Before doing this we derive a simplified analytical model to understand easily some aspects of the solutions.

2.4 Asymptotic shapes and expressions for the XPW spectrum

If we assume a sufficiently regular and smooth input spectrum (i.e., not necessarily a Gaussian pulse), some features of the XPW spectrum can be described by applying the stationary phase theorem to expression (7). This theorem leads, as we will discuss later, to two different results with two different and complementary ranges of validity. The goal of this model is to understand in a simple way the influence of the residual phase on the XPW spectrum and so to extract an information of this phase from the shape of this spectrum. The results of the asymptotic model are confirmed more quantitatively by the numerical calculation. Before entering the heart of the matter, we first recall the stationary phase theorem applied to a bidirectional complex function of modulus $a(x, y)$ and phase $\phi(x, y)$. According to the stationary phase theorem, the main contribution terms of the integral

$$\int_{\mathbb{R}^2} a(x, y) e^{i\phi(x, y)} dx dy \tag{13}$$

come from the angular frequencies x_0 and y_0 for which the phase of the integrand is locally stationary. If such stationary point exists in the $[x_0, y_0]$ ensemble for a particular value of ω_c , then the XPW spectrum will exhibit a local maximum at angular frequency ω_c . What is more, the theorem also gives the following asymptotic formula when the phase is locally stationary ($\phi'(x_0, y_0) = 0$) but not critical ($\phi''(x_0, y_0) \neq 0$):

$$\int_{\mathbb{R}^2} a(x, y)e^{i\phi(x,y)/h} dx dy = 2\pi \frac{a(x_0, y_0)e^{i\phi(x_0,y_0)/h}}{\sqrt{|\phi_{x,x}\phi_{y,y} - \phi_{x,y}\phi_{y,x}|/h}} e^{i\frac{\pi}{4} \text{sign}\phi''(x_0,y_0)} + O(h^2). \tag{14}$$

Moreover, in this section and in the following sections, the central angular frequency and spectral width of the cube of the input spectral intensity will be denoted $\langle \omega \rangle_{I_A^3}$ and $\sigma_{I_A^3}$, respectively.

2.4.1 Spectral phase with critical points

Mathematically, the stationary phase condition applied to the integrand of the right hand side of (7) is:

$$\exists (\omega_1, \omega_2) \left| \frac{d}{d\omega_{1,2}} [\varphi(\omega_1) + \varphi(\omega_2) - \varphi(\omega_1 + \omega_2 - \omega)] \right. \\ \left. = f_{1,2}(\omega), \tag{15} \right.$$

where $f_{1,2}(\omega)$ are two real functions. This condition of local maximum has a more natural expression using the group delays:

$$\begin{cases} \tau(\omega_1) - \tau(\omega_1 + \omega_2 - \omega) = f_1(\omega), \\ \tau(\omega_2) - \tau(\omega_1 + \omega_2 - \omega) = f_2(\omega). \end{cases} \tag{16}$$

Although the exact set of solutions of this equation system is unknown in the general case, there is one obvious solution: $\omega_1 = \omega_2 = \omega$. If this solution is the only solution, then, an asymptotic expression of the XPW spectrum is:

$$I_B(\omega) \simeq \frac{I_A(\omega)^3}{|\varphi''(\omega)|^2}. \tag{17}$$

From a mathematical point of view, the range of validity of the stationary phase is limited to high phase values, that is to say for input pulses which are far from the Fourier-transform limit. Nevertheless, this approximation proves useful. If the fundamental spectral phase exhibits a critical point ($\varphi''(\omega_c) = 0$), then the phase function of (7) is also critical at ω_c and formula (17) cannot be applied around ω_c , which is obvious since the formula diverges at ω_c . However, in such a case, the XPW spectrum can still be described by the sum of two contributions: a “local” contribution given by expression (17) (away from ω_c) and a “critical” contribution corresponding to a peak distribution located at ω_c .

An example of this is a spectral phase well described by a third order Taylor expansion around ω_0 , then the XPW spectrum is expected to exhibit a maximum at the angular frequency which is a solution of:

$$\varphi''(\omega) = \varphi^{(2)} + \varphi^{(3)}(\omega - \omega_0) = 0. \tag{18}$$

This analytical approach enables us to predict the following spectral behavior of the XPW spectrum: when there are strong residual second and third order phases on the fundamental pulse, the XPW spectrum is no longer symmetric even for a symmetric input. What is more, the XPW spectrum is the sum of the cube of the input spectrum and a peak at the position:

$$\omega = \omega_0 - \frac{\varphi^{(2)}}{\varphi^{(3)}}. \tag{19}$$

Since the peak distribution is weighted by the amplitude factor I_A^3 , the spectral center of mass is therefore expected to behave as follows:

$$\langle \omega \rangle_{\text{XPW}} = \omega_0 - \frac{\varphi^{(2)}}{\varphi^{(3)}} I_A^3(\omega_0 - \varphi^{(2)}/\varphi^{(3)}) / I_A^3(\omega_0). \tag{20}$$

In this particular case, the range of validity of this approximation can be defined as $\sigma_{I_A^3}^3 |\varphi^{(3)}| \gg 1$ and $|\varphi^{(2)}| < |\varphi^{(3)}\sigma|$.

2.4.2 Spectral phase without critical points

The stationary phase theorem gives also some asymptotic expressions for the XPW spectrum when there are no critical points for the fundamental pulse. More precisely, if the group delay of the input pulse is monotonic (this is the case if the spectral phase is predominantly quadratic or quartic, for example) and if the duration of the fundamental pulse is much longer than its transform-limit, then the XPW modulus of the spectral amplitude is approximately given by the solution in (17), over the whole spectral range.

From this result one can compute, to the first order, the spectral center of mass and spectral width of the XPW spectrum for a chirped input pulse to which a perturbative third order phase has been added:

$$\langle \omega \rangle_{\text{XPW}} = \omega_0 - 2 \frac{\varphi^{(3)}}{\varphi^{(2)}} \sigma_{I_A^3}^2, \tag{21}$$

$$\sigma_{\text{XPW}}^2 = \sigma_{I_A^3}^2 - 2 \frac{\varphi^{(3)}}{\varphi^{(2)}} \langle (\omega - \omega_0)^3 \rangle_{I_A^3}. \tag{22}$$

Applying this result to a linearly chirped pulse ($\varphi^{(3)} = 0$), leads to the same results found in Sect. 2.3 for large chirps: the spectrum is narrowed by a factor $\sqrt{3}$, the conversion efficiency decreases with $1/(\varphi^{(2)})^2$. With a perturbative third order phase, the spectral center of mass is shifted proportionally to the $\varphi^{(3)}$ value. As far as the spectral width is concerned, it remains unchanged to the first order if the spectrum is symmetric with respect to the spectral center of mass. If the spectrum is not symmetric, then the spectrum may be broadened or narrowed depending on the relative signs of the phase coefficients.

Again, the range of validity of these approximations needs to be specified. The above results only apply for

strongly chirped pulses. For a general cubic phase function, this means $\sigma_{IA}^2 |\varphi^{(2)}| \gg 1$ and $|\varphi^{(2)}| \gg |\varphi^{(3)} \sigma_{IA}|$.

2.4.3 Synthesis

This very simplified model predicts that, for a sufficiently regular spectrum with a large general cubic phase, the spectral center of mass varies linearly with $\varphi^{(3)}$ for large and constant values of $\varphi^{(2)}$ and linearly with $\varphi^{(2)}$ for large and constant values of $\varphi^{(3)}$. Such features are characteristic of a hyperbolic parabola surface, more widely known as a horse saddle surface. This saddle point is centered at $\varphi^{(2)} = \varphi^{(3)} = 0$ and can be implicitly defined by the equation $\varphi^{(2)}\varphi^{(3)} = cte$. The spectral width of the XPW spectrum is expected to be almost constant whenever the effects of $\varphi^{(2)}$ or $\varphi^{(3)}$ are dominant. In the first case, the spectral width is equal to that of the cube of the input spectrum. In the second case, it is related to the spectral width of the “critical” contribution. Last, this model confirms a general Lorentzian dependence of the XPW spectrum as a function of $\varphi^{(2)}$.

2.5 Numerical calculation

In this section we directly solve (7) and compute the XPW spectral intensity without any other assumptions than those stated in Sect. 2.2. In order to verify the previous theoretical work, we simulate the effect of combined second and third order spectral phases. The input spectrum is Gaussian with a spectral width corresponding to a Fourier transform limited pulse of 30 fs. The energy, center of mass and spectral width of the XPW spectrum are shown in Figs. 1 and 2. For all these scans we choose approximately $\Delta\varphi^{(2)} = \sigma_{IA}^2 \Delta\varphi^{(3)}$.

The main conclusion from Fig. 1 is that the plots are symmetric with respect to the point where $\varphi^{(2)} = \varphi^{(3)} = 0$. At this point the XPW generation process exhibits maximum efficiency and the broadest spectrum without spectral shift. Efficiency and broadening decrease with residual spectral phase and we obtain numerically the same values for $\varphi_{cr,Energy}^{(2)}$ and $\varphi_{cr,Width}^{(2)}$ that we have previously derived analytically. As expected, the spectral center of mass of the XPW spectrum (Fig. 2(a)) shifts when the contributions of second and third order phase coefficients are of the same order of magnitude. The numerical calculations provide realistic spectral shift that can be used to compare with experimental data. For comparison, we are presenting, in Fig. 2(b), the spectral shift behavior extracted from the analytical model for the same spectral phase range as Fig. 2(a). They both behave the same, but the numerical calculations provide realistic spectral shift for Gaussian laser spectra compared to the analytical model. Furthermore, the analytical model is not valid at the saddle point in the center of the graph.

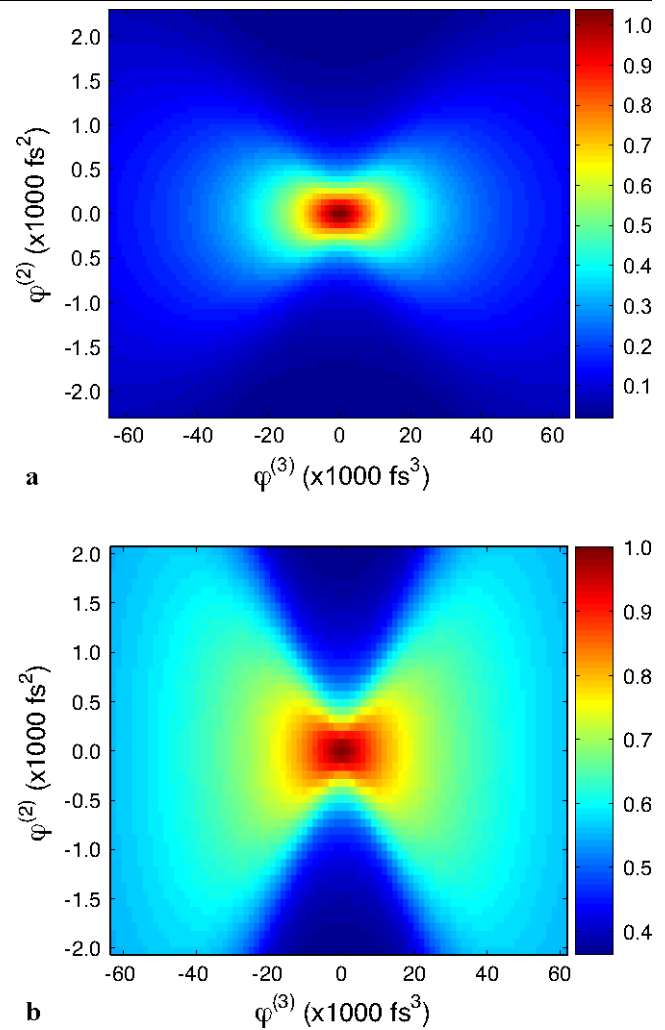
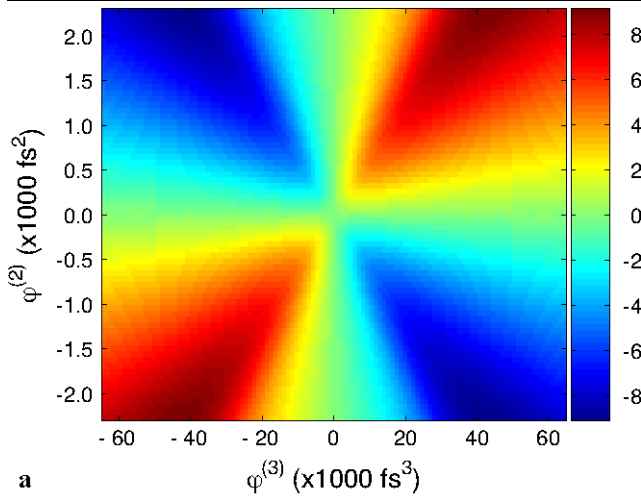


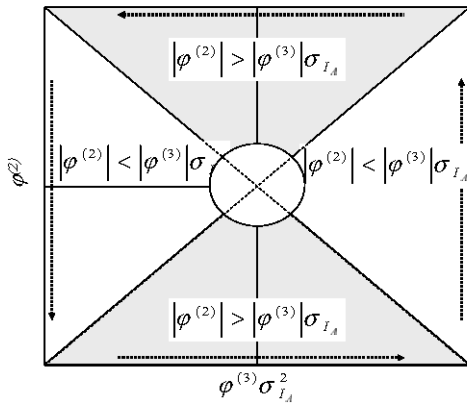
Fig. 1 (a) Normalized theoretical XPW efficiency function of the second and third order spectral phase for a 30 fs input pulse. The value 1 corresponds to a XPW efficiency of 5%. (b) Theoretical prediction of XPW spectral width as a function of the second and third order spectral phases for a 30 fs pulse. The spectral width values are normalized to the XPW width value for the case of transform limited input pulse

3 Experimental results

The XPW experimental setup is shown in Fig. 3. We use a commercial femtosecond laser (Femtolasers GmbH) delivering 1 mJ, 30 fs pulses at 1 kHz. The spectral phase of the compressed pulses was measured with an homemade SPIDER [20] and corrected using an acousto-optical programmable dispersive filter (AOPDF, Dazzler™ [21]) inserted into the chirped pulse amplifier. By doing so we have noticed that we removed $\varphi^{(4)} \sim -2 \times 10^6 \text{ fs}^4$ and $\varphi^{(5)} \sim 50 \times 10^6 \text{ fs}^5$. Furthermore, in order to test the effect of remaining spectral phase higher order terms, we can cancel the Dazzler correction and make experiment with known $\varphi^{(4)}$ and $\varphi^{(5)}$ values. Those high order phase values are considered typical for 30 fs laser systems.



a



b

Fig. 2 (a) Theoretical prediction of the XPW spectral center of mass shift (in nm) as a function of the second and third order spectral phases for a 30 fs input pulse. (b) Validity range of the two approximations in the $(\varphi^{(2)}(\omega_0), \varphi^{(3)}(\omega_0))$ plane for the analytical model. The arrows show the direction of the spectral center of mass shift for a cubic spectral phase

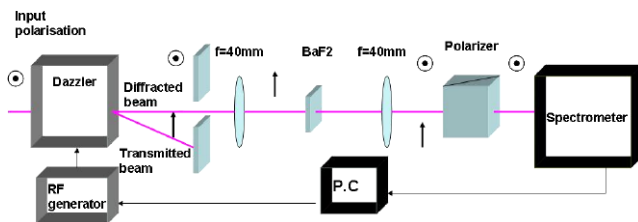


Fig. 3 Experimental setup

To study experimentally the effect of the spectral phase on the XPW process, we use a second AOPDF (25 mm TeO₂ crystal) as a versatile and precise way to tune the spectral phase on demand. This AOPDF is placed between the laser and the XPW setup. To avoid damaging the AOPDF, we only use 1 μ J from the total laser energy for our experiments. The diffracted output of the AOPDF is focused by a 40 mm focal length achromatic lens into a 1 mm thick BaF₂ crystal, the XPW beam is selected through a polarizer and fo-

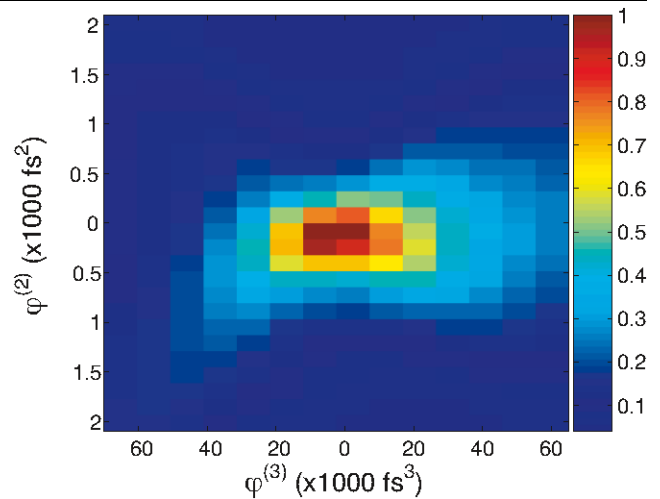


Fig. 4 Experimental 2D plot of the normalized XPW efficiency versus $\varphi^{(2)}$ and $\varphi^{(3)}$ after compensation of the higher order spectral phase terms. The value 1 corresponds to a XPW efficiency of 5%

cused down on the entrance slit of a spectrometer (Avantes). Both AOPDF and spectrometer were synchronized with the laser pulse. The spectral phase from the laser was considered flat, except for the cases when we deliberately introduce the known higher order residual phase. The AOPDF was first set to compensate both its own dispersion and that of the focusing lens in a static way. We then use the AOPDF to add to the optical pulse some user-defined spectral phase. In the experiments presented we added the following spectral phases:

$$\delta\varphi(\omega) = \varphi^{(2)}(\omega - \omega_0)^2/2 + \varphi^{(3)}(\omega - \omega_0)^3/6. \quad (23)$$

Both coefficients $\varphi^{(2)}$ and $\varphi^{(3)}$ were automatically scanned between -2000 and $+2000$ fs² for $\varphi^{(2)}$ (32 points) and between -60000 and $+60000$ fs³ for $\varphi^{(3)}$ (16 points). For each $\delta\varphi(\omega)$, a different acoustic wave was loaded into the AOPDF generator and the XPW spectrum was recorded and processed. With this setup, a systematic experimental analysis of the effect of cubic spectral phases on the XPW spectrum and efficiency was made possible.

3.1 XPW efficiency

We first consider the effect of spectral phase on XPW efficiency. As the input energy is constant, the XPW efficiency is proportional to the XPW output energy. Therefore, the XPW efficiency is obtained by integrating every acquired XPW spectrum over the whole spectral range. Figure 4 shows the obtained experimental efficiency map that should be compared with the theoretical map shown in Fig. 1. In both cases, there is a global maximum of the efficiency corresponding to $\varphi^{(2)} = \varphi^{(3)} = 0$. This is due to the fact that XPW (as all nonlinear effects) is highly sensitive to peak intensity and the highest peak intensity is obtained for a pulse

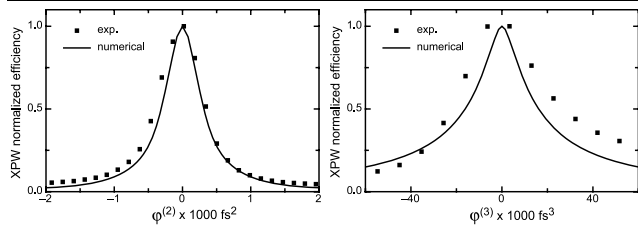


Fig. 5 Left: normalized experimental (points) (dashed line) and theoretical Lorentzian (solid line) XPW efficiency as a function of $\varphi^{(2)}$ for $\varphi^{(3)} = 0$. Right: normalized experimental points and theoretical (solid line) XPW efficiency as a function of $\varphi^{(3)}$ for $\varphi^{(2)} = 0$

with a flat spectral phase. In Fig. 5 we plot cross sections of this map for $\varphi^{(3)} = 0 \text{ fs}^3$ and for $\varphi^{(2)} = 0 \text{ fs}^2$. The theoretical curves are obtained from the same cross sections of Fig. 1(a). As predicted, the efficiency decreases with second order phase with a Lorentzian dependence. In particular, we obtain that the experimental $\varphi_{\text{cr,Energy}}^{(2)} = +350 \text{ fs}^2$ corresponds to the theoretical one. The variation of the XPW efficiency with third order spectral phase fits with numerical calculation. The difference between the two curves is due to the imprecision of the measurement and correction of high order spectral phase terms.

In the case of a laser pulse with a residual spectral phase ($\varphi^{(4)} \sim -2 \times 10^6 \text{ fs}^4$ and $\varphi^{(5)} \sim 50 \times 10^6 \text{ fs}^5$) we obtain an asymmetric efficiency dependence on $\varphi^{(2)}$ and $\varphi^{(3)}$ (Fig. 6). This behavior can be reproduced numerically. To center the map, both coefficients $\varphi^{(2)}$ and $\varphi^{(3)}$ were scanned between -1500 and $+4000 \text{ fs}^2$ for $\varphi^{(2)}$ and between -80000 and $+80000 \text{ fs}^3$ for $\varphi^{(3)}$. The asymmetry can be explained intuitively. When $\varphi^{(2)}$ reaches a value corresponding to the opposite of the residual $\varphi^{(4)}$ value, the effects of both phase terms mutually compensate, yielding better efficiency. When $\varphi^{(2)}$ and $\varphi^{(4)}$ have the same sign the effects of both phase terms sum up. This gives the vertical asymmetry in Fig. 6. The horizontal asymmetry is due to the same combination of effects between $\varphi^{(3)}$ and $\varphi^{(5)}$. Furthermore, maximum efficiency (which is less than in the case of a perfect flat phase) is reached at a non-zero $[\varphi^{(2)}, \varphi^{(3)}]$ where the input spectral phase is the flattest.

3.2 Spectral width

We now consider the effect of spectral phase on the XPW generated spectral width. Figure 7 shows the map displaying the spectral width of the previously acquired spectra. These data have been obtained with a laser pulse uncorrected for higher order spectral phase terms, so the theoretical curve in Fig. 7 is calculated using $\varphi^{(4)} \sim -2 \times 10^6 \text{ fs}^4$ and $\varphi^{(5)} \sim 50 \times 10^6 \text{ fs}^5$.

It can be noticed again that there is a global maximum of the spectral width when the total spectral phase is almost flat since both the efficiency and the spectral width reach

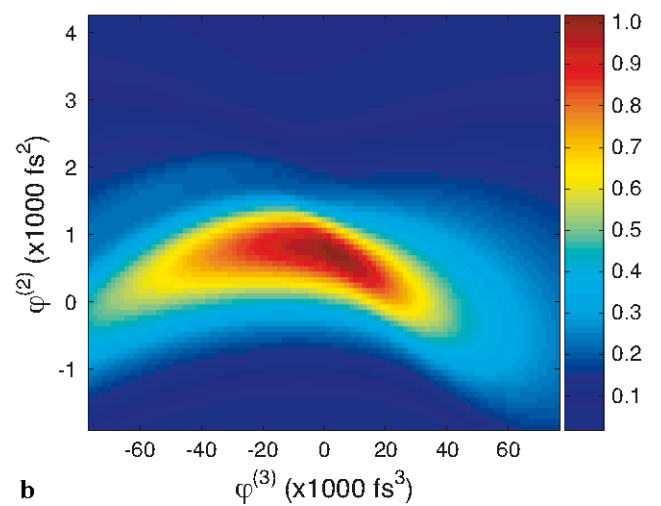
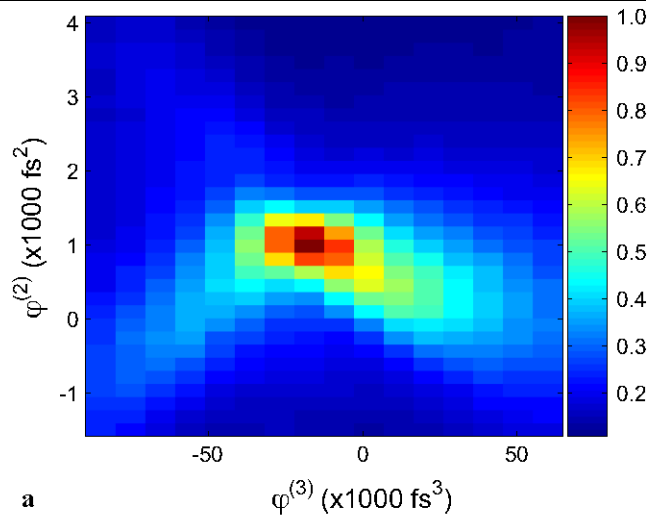


Fig. 6 Experimental (a) and theoretical (b) 2D plot of the normalized XPW efficiency versus $\varphi^{(2)}$ and $\varphi^{(3)}$ with known residual $\varphi^{(4)}$ and $\varphi^{(5)}$

their maximum for the same $(\varphi^{(2)}, \varphi^{(3)})$. The asymmetry of the maps in Fig. 7 is very similar to that already discussed for the efficiency map. As previously this can be explained by the residual higher order spectral phase. The value for $\varphi_{\text{cr,Width}}^{(2)}$ derived experimentally is comparable to the numerical prediction.

3.3 Spectral shift

The last parameter that we considered is the shift of the center of mass of the XPW spectrum. As shown previously, a shifted spectral center of mass means an imperfect compression of the input pulse

Figure 8(a) shows the center of mass shift of the XPW spectrum as a function of $[\varphi^{(2)}, \varphi^{(3)}]$ in the case of uncompensated higher order spectral phase terms. This map is in agreement with the hyperbolic parabola derived in the case of a pure $\varphi^{(2)}, \varphi^{(3)}$ scan. The analytical model

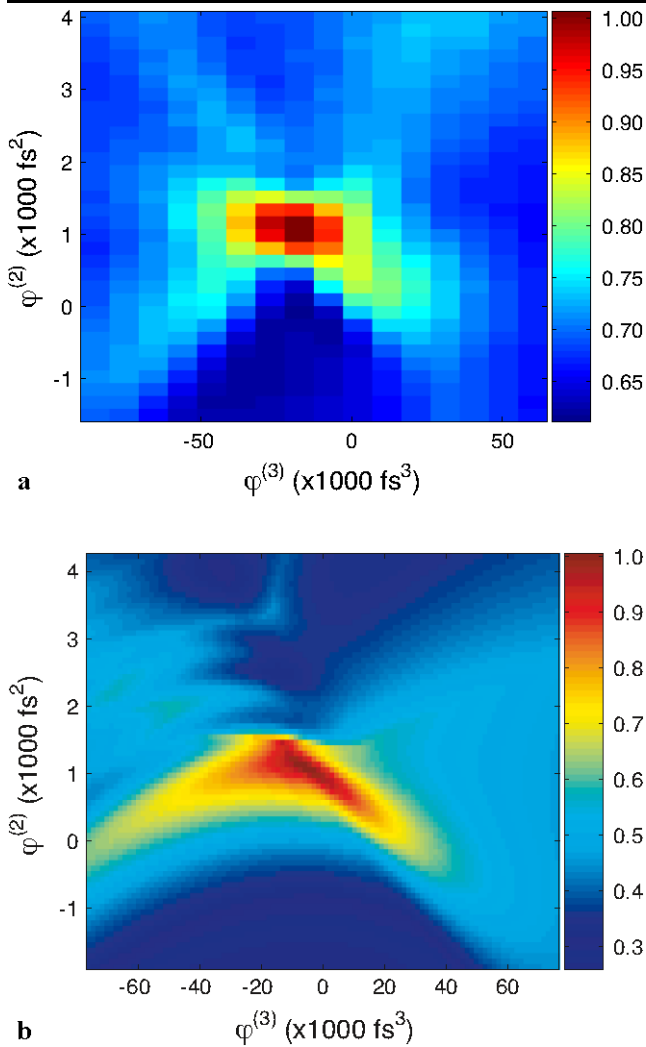


Fig. 7 Experimental (a) and theoretical (b) 2D plot of the XPW pulse spectral width versus $\varphi^{(2)}$ and $\varphi^{(3)}$. The spectral width values are normalized to the maximum (best compression of the input pulse) of the 2D plot

we have derived in the theoretical section tells us that for a residual $\varphi^{(2)}$ and $\varphi^{(3)}$ the spectrum becomes asymmetric.

It also indicates that for a fixed and large value of $\varphi^{(3)}$, the center of mass shifts linearly with $\varphi^{(2)}$. The sign of the slope of this curve depends on the sign of $\varphi^{(3)}$. This is confirmed by experiments (Fig. 9) in the zone where this approximation is valid. It can also be noticed that this linear shift does not continue indefinitely for larger values of $\varphi^{(2)}$. By changing the input cubic spectral phase we obtain a global shift of the center of mass which is at maximum 1/3 of the spectral bandwidth. The shift of the XPW spectral center of mass function of $\varphi^{(2)}$ for two symmetrical values of $\varphi^{(3)}$ is not perfectly symmetric (for example, see Fig. 9) due to the higher order residual phase terms.

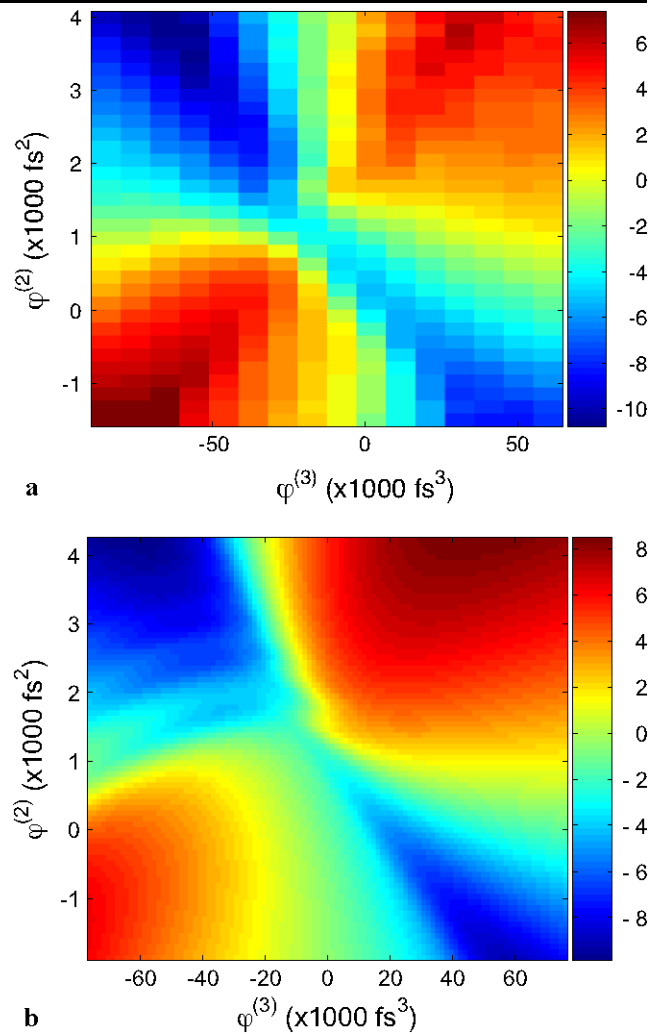


Fig. 8 Experimental (a) and theoretical (b) 2D plot of XPW spectra center of mass shift (in nm) versus $\varphi^{(2)}$ and $\varphi^{(3)}$ with known residual $\varphi^{(4)}$ and $\varphi^{(5)}$

If we compare Figs. 2(a) and 8(a) around the zone of optimum input pulse compression (saddle point) we see that the experimental map has an additional shift towards short wavelength compared to the theoretical one. Repeating simulation with the residual $\varphi^{(4)}$ and $\varphi^{(5)}$ spectral phase mentioned previously, we obtained this spectral shift as is shown in Fig. 8(b). The center of mass of the XPW spectrum is visibly influenced by the higher order spectral phase also near $\varphi^{(2)} = \varphi^{(3)} = 0$ with a shift towards shorter wavelengths when $\varphi^{(4)}$ and $\varphi^{(5)}$ are of opposite sign, and towards longer wavelengths when they are of the same sign. Therefore, higher order spectral phase terms have an influence on the XPW signal for any values of $[\varphi^{(2)}, \varphi^{(3)}]$. They shift the central wavelength, and influence the XPW efficiency and spectral width for higher values of $\varphi^{(2)}$ and $\varphi^{(3)}$.

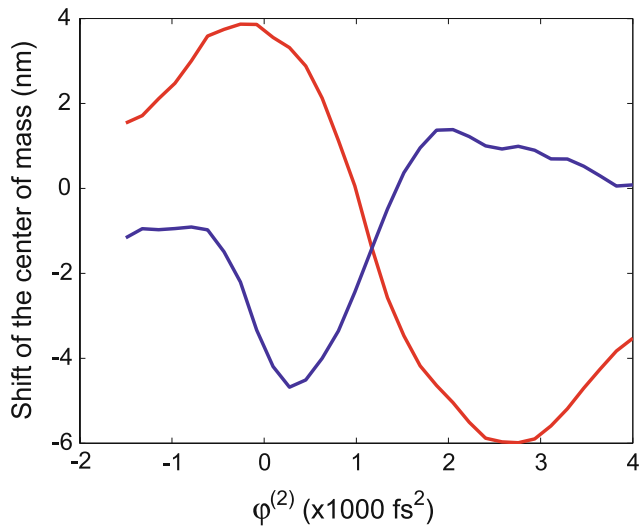


Fig. 9 Shift of the XPW spectra center of mass as a function of $\varphi^{(2)}$ for $\varphi^{(3)} = -20000 \text{ fs}^3$ (red) and $\varphi^{(3)} = +20000 \text{ fs}^3$ (blue)

4 Practical experimental conditions for XPW generation

From this systematic theoretical and experimental analysis we get a general idea of the role of the spectral phase on the XPW nonlinear process. In particular, we extract experimentally the maximum tolerable values of residual spectral phase for an input pulse of 30 fs. We have demonstrated that it is fundamental to compensate at least a pure second order spectral phase to a residual value lower than $\pm 325 \text{ fs}^2$ and the pure third order phase to a residual value lower than $\pm 17500 \text{ fs}^3$ if we want to obtain half of the maximum XPW efficiency. In this range the XPW spectrum is broadened and the center of mass is shifted at maximum by 4 nm compared to the fundamental which is perfectly adapted for amplification in a Ti:Sa amplifier. These values of spectral phase are slightly increased ($\pm 500 \text{ fs}^2$ and $\pm 25000 \text{ fs}^3$) when residual higher order spectral phase terms are present. This can be understood as, for a spectral phase with some residual higher order terms, the XPW signal is lower than the one obtained for a perfectly compressed pulse. Those spectral phase higher order terms can be compensated by a wide combination of second and third order terms. Therefore, it is broadening the region for which the XPW efficiency is kept above half of the maximum efficiency. In this case there is a shift of the center of mass even with a perfect compensation of the $\varphi^{(2)}$ and $\varphi^{(3)}$ terms. These values agree with our numerical simulations.

For a given stretcher compressor system, those $\varphi^{(2)}$ and $\varphi^{(3)}$ values can be correlated to a range of acceptable grating spacing variation and a range of incident angle variations that preserve an efficient XPW generation. Those ranges can also be seen as the degree of precision needed for the given

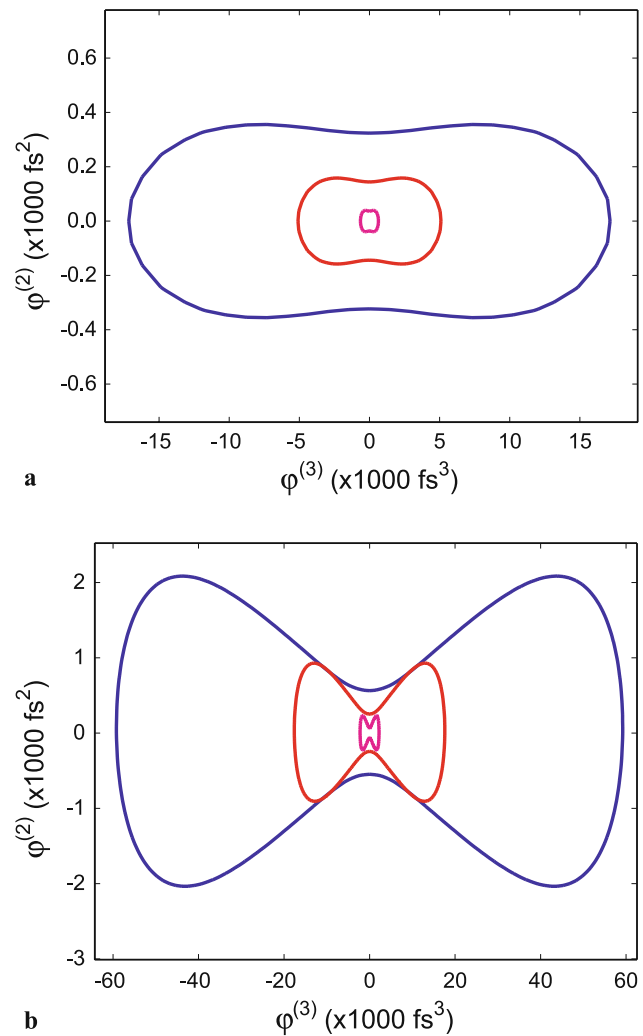


Fig. 10 (a) Contour line representing the maximum values of $\varphi^{(2)}$ and $\varphi^{(3)}$ to obtain half of the maximum XPW efficiency for 30 fs (blue), 20 fs (red), and 10 fs (purple) input pulse duration, respectively. (b) Contour line representing the maximum values of $\varphi^{(2)}$ and $\varphi^{(3)}$ to obtain $\Delta\lambda_{\text{XPW}} = \Delta\lambda_{\text{laser}}$ for 30 fs (blue), 20 fs (red), and 10 fs (purple) input pulse duration, respectively. The range of both axis is different for the two figures, i.e., the areas in (a) are broader than the corresponding areas in (b)

stretcher compressor system to allow an efficient XPW generation.

As this range of $\varphi^{(2)}$ and $\varphi^{(3)}$ values for efficient XPW generation is of the same order of magnitude as the measurement precision obtained with a FROG or a SPIDER, the best approach is to tune the stretcher compressor system to the optimum and then tune the compressor slightly to optimize the XPW generation efficiency without spectral shift.

We can next generalize this analysis to shorter input pulse durations. This is important as it allows us to know in general, when the input pulse can be defined as “Fourier limited” with respect to the XPW generation process. Figure 10(a) shows the $[\varphi^{(2)}, \varphi^{(3)}]$ area for which efficiency is

reduced by less than half calculated for 30, 20, and 10 fs pulses. The elongated peanut shape of these areas is due to partial compensation between $\varphi^{(2)}$ and $\varphi^{(3)}$ which induces a partially flat spectral phase preventing excessive stretching of the pulse. Higher order phase terms break the symmetry of these plots and can also be evaluated theoretically. From this figure we confirm how fast the acceptable area decreases with the decreasing input duration.

We demonstrated in [10] that the chirp of the generated XPW pulse is reduced up to 9 times compared to the incident pulse chirp. This improvement is getting less with the increase of the input chirp and reaches a value equal to the input one for large values of input chirp. This behavior can be extended for higher order phase terms as has been done for second order nonlinearities [19]. Therefore, we can predict that the spectral phase of the XPW pulse is flattened for the values of $\varphi^{(2)}$ and $\varphi^{(3)}$ yielding good XPW efficiency (i.e., in the area defined by Fig. 10(a)). This area is the one typically used for contrast improvement with XPW, and corresponds to the area where XPW also improves the coherent contrast of the pulse [4]. Outside this area the XPW spectral phase corresponds to the input pulse spectral phase.

Figure 10(b) shows the $[\varphi^{(2)}, \varphi^{(3)}]$ area that preserves the initial spectral width of the laser for the same input pulse durations. As we can observe, this area is broader than the area for efficient XPW generation (Fig. 10(a)). XPW spectra generated for a couple $[\varphi^{(2)}, \varphi^{(3)}]$ at the border of this area are modulated by the conversion of the input spectral phase to the spectral amplitude by the XPW nonlinear process. This effect could allow approximate spectral tailoring in some coherent control experiments. This is emphasized by the fact that the main feature of the tailoring using the spectral phase is a controllable central wavelength shift.

5 Conclusions

In this paper we demonstrate the importance of controlling the spectral phase of the input pulse for a correct generation of Cross Polarized Wave with sub-30 fs pulses and how to optimize the pulse compression after the first CPA directly with the nonlinear effect of the XPW filter. With this control the XPW filter maintains all its benefits (increasing of ns and ps temporal contrast, spectral broadening) for pulses as short as 10 fs.

Figure 11 shows a 85 nm XPW spectrum obtained from a 47 nm input spectrum. The compression of the input pulse was optimized with the Dazzler to obtain a transform limited pulse. The XPW spectrum is Gaussian, broadened by a factor $\sqrt{3}$ and centered at the same wavelength as the input pulse. Following the discussion presented in this paper this demonstrates the optimal compression of the input beam. It is important to notice that, due to the spectral filtering,

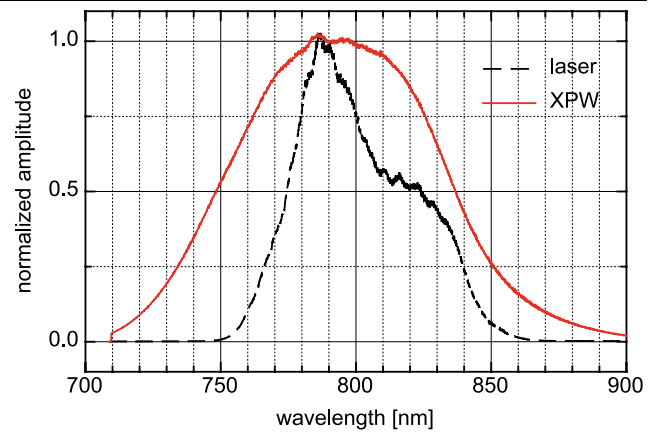


Fig. 11 Spectrum of the input pulse (black) and of the XPW generated pulse (red). The XPW spectrum is Gaussian, broadened by a factor $\sqrt{3}$ and centered at the same wavelength as the input pulse giving a FWHM of about 85 nm. The input pulse is optimally compressed with a Dazzler

the XPW spectrum is Gaussian even with a modulated input spectrum. This feature can be very useful for sub-10 fs pulses as they usually exhibit modulated spectral amplitude and phase. Perfectly compressed and filtered by XPW generation such spectra could be transformed in pedestal free sub-10 fs Gaussian spectrum pulses which can be further amplified in an OPCPA system.

Acknowledgements Financial support from the Agence Nationale pour la Recherche, through programs BLAN06-3_134072 (ILAR) and Chaire d'Excellence 2004, is gratefully acknowledged. S.M. Saltiel, S. Kourtev and N. Minkovski acknowledge the support of Extreme Light Infrastructure project (grant No. 212105).

References

1. N. Minkovski, G.I. Petrov, S.M. Saltiel, O. Albert, J. Etchepare, *J. Opt. Soc. Am. B* **21**, 1659 (2004)
2. A. Jullien, O. Albert, F. Burgy, G. Hamoniaux, J.-P. Rousseau, J.-P. Chambaret, F. Augé-Rochereau, G. Chériaux, J. Etchepare, N. Minkovski, S.M. Saltiel, *Opt. Lett.* **30**, 920 (2005)
3. V. Chvykov, P. Rousseau, S. Reed, G. Kalinchenko, V. Yanovsky, *Opt. Lett.* **31**, 1456 (2006)
4. L. Canova, M. Merano, A. Jullien, G. Chériaux, R. Lopez-Martens, O. Albert, N. Forget, S. Kourtev, N. Minkovski, S.M. Saltiel, in *Conference on Lasers and Electro-Optics/Quantum Electronics and Laser Science Conference and Photonic Applications Systems Technologies*, JThD131 (2007)
5. M. Kalashnikov, K. Osvay, W. Sandner, *Laser Part. Beams* **25**, 219 (2007)
6. M.P. Kalashnikov, K. Osvay, I.M. Lachko, H. Schönagel, W. Sandner, *Appl. Phys. B* **81**, 1059 (2005)
7. T. Oksenhendler, D. Kaplan, P. Tourmois, G.M. Greetham, F. Estable, *Appl. Phys. B* **83**, 491 (2006)
8. H. Takada, K. Torizuka, *IEEE J. Sel. Top. Quantum Electron.* **12**, 201 (2006)
9. I. Pastirk, B. Resan, A. Fry, J. MacKay, M. Dantus, *Opt. Express* **14**, 9537 (2006)

10. A. Jullien, L. Canova, O. Albert, D. Boschetto, L. Antonucci, Y.-H. Cha, J.P. Rousseau, P. Chaudet, G. Chériaux, J. Etchepare, S. Kourtev, N. Minkovski, S.M. Saltiel, *Appl. Phys. B* **87**, 595 (2007)
11. M.P. Kalashnikov, E. Risse, H. Schönngel, W. Sandner, *Opt. Lett.* **30**, 923 (2005)
12. M.E. Anderson, L.E.E. de Araujo, E.M. Kosik, I.A. Walmsley, *Appl. Phys. B* **70**, S85 (2000)
13. D.N. Fittinghoff, K.W. DeLong, R. Trebino, C.L. Ladera, *J. Opt. Soc. Am. B* **12**, 1955 (1995)
14. G. Stibenz, C. Ropers, C. Lienau, C. Warmuth, A.S. Wyatt, I.A. Walmsley, G. Steinmeyer, *Appl. Phys. B* **83**, 511 (2006)
15. E. Sidick, A. Dienes, A. Knoesen, *J. Opt. Soc. Am. B* **12**, 1713 (1995)
16. A.C.L. Boscheron, C.J. Sauteret, A. Migus, *J. Opt. Soc. Am. B* **13**, 818 (1996)
17. K. Osvay, I.N. Ross, *J. Opt. Soc. Am. B* **13**, 1431 (1996)
18. G. Veitas, R. Danielius, *J. Opt. Soc. Am. B* **16**, 1561 (1999)
19. P. Baum, S. Lochbrunner, E. Riedle, *Appl. Phys. B* **79**, 1027 (2004)
20. C. Iaconis, I.A. Walmsley, *Opt. Lett.* **23**, 792 (1998)
21. F. Verluise, V. Laude, Z. Cheng, C. Spielmann, P. Tournois, *Opt. Lett.* **25**, 575 (2000)